Article

Conformational Dynamics of the Nicotinic Acetylcholine Receptor Channel: A 35-ns Molecular Dynamics Simulation Study

Yechun Xu, Francisco J. Barrantes, Xiaomin Luo, Kaixian Chen, Jianhua Shen, and Hualiang Jiang

J. Am. Chem. Soc., **2005**, 127 (4), 1291-1299• DOI: 10.1021/ja044577i • Publication Date (Web): 08 January 2005

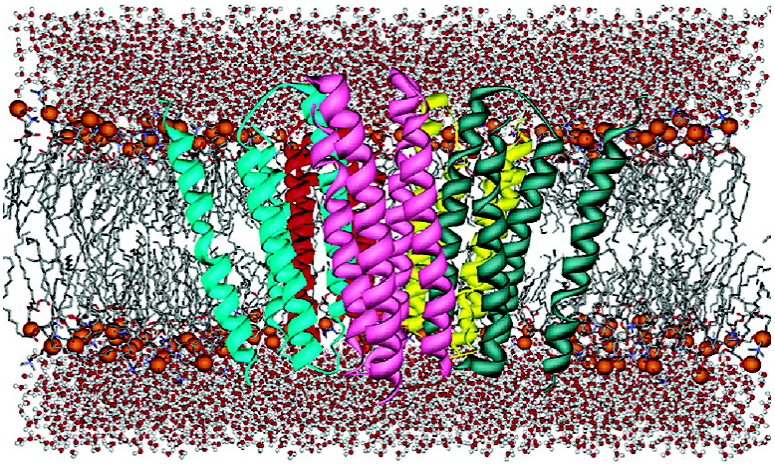

J|A|C|S
ARTICLES
Published on Web 01/08/2005

Conformational Dynamics of the Nicotinic Acetylcholine Receptor Channel: A 35-ns Molecular Dynamics Simulation Study

Yechun Xu,[†] Francisco J. Barrantes,[‡] Xiaomin Luo,[†] Kaixian Chen,[†] Jianhua Shen,*[,†] and Hualiang Jiang*[,†,§]

Contribution from the Center for Drug Discovery and Design, State Key Laboratory of Drug Research, Shanghai Institute of Materia Medica, Shanghai Institutes for Biological Sciences, and Graduate School, Chinese Academy of Sciences, 555 Zuchongzhi Road, Shanghai 201203, China, Instituto de Investigaciones Bioquímicas de Bahía Blanca and UNESCO Chair of Biophysics & Molecular Neurobiology, CC 857, B8000FWB, Bahía Blanca, Argentina, and School of Pharmacy, East China University of Science and Technology, Shanghai 200237, China

Received September 8, 2004; E-mail: hljiang@mail.shcnc.ac.cn

Abstract: The nicotinic acetylcholine receptor (AChR) is the paradigm of ligand-gated ion channels, integral membrane proteins that mediate fast intercellular communication in response to neurotransmitters. A 35-ns molecular dynamics simulation has been performed to explore the conformational dynamics of the entire membrane-spanning region, including the ion channel pore of the AChR. In the simulation, the 20 transmembrane (TM) segments that comprise the whole TM domain of the receptor were inserted into a large dipalmitoylphosphatidylcholine (DPPC) bilayer. The dynamic behavior of individual TM segments and their corresponding AChR subunit helix bundles was examined in order to assess the contribution of each to the conformational transitions of the whole channel. Asymmetrical and asynchronous motions of the M1−M3 TM segments of each subunit were revealed. In addition, the outermost ring of five M4 TM helices was found to convey the effects exerted by the lipid molecules to the central channel domain. Remarkably, a closed-to-open conformational shift was found to occur in one of the channel ring positions in the time scale of the present simulations, the possible physiological significance of which is discussed.

Introduction

The nicotinic acetylcholine receptor (AChR) is the best-characterized member of the ligand-gated ion channel superfamily.[1] In embryonic receptor in muscle or in the adult form in electrocytes, the AChR is a hetero-pentameric protein composed of four homologous subunits in a stoichiometry $\alpha_2\beta\gamma\delta$. Each subunit contains four transmembrane (TM) segments (M1−M4), which constitute the membrane-embedded region of the protein. The TM segments are connected by loops. As shown in Figure 1A, the innermost ring of five M2 segments, one from each subunit, constitutes the walls of the AChR ion channel pore.[2] The other TM segments, M1 and M3, form an intermediate ring in contact with the five M2 segments and with the outermost ring of five M4 segments; the latter ring is directly in contact with the surrounding lipid phase.[2]

The structure of the AChR ion channel has been extensively studied using experimental and computational approaches.[1,3−5] The four membrane-spanning segments were initially assumed to be α-helical.[4,5] Subsequent cryoelectron microscopy studies of the AChR at 9-Å resolution,[6] molecular modeling[7] and secondary structure predictions[8] led to the postulation that the TM region of the AChR adopts a predominantly mixed α/β topology. It was also hypothesized that the β-strands in M1, M3, and M4 formed a β-barrel surrounding five M2 α-helices. However, the first atomic structure of the whole TM domain of the AChR recently determined by cryoelectron microscopy at 4-Å resolution suggests that all the TM segments are helical and adopt the antiparallel α-helical bundle motif.[9]

The function of the AChR ion channel is the permeation of cations. Binding of acetylcholine to the extracellular domain of the receptor triggers the opening of the ion channel located in the TM region, which allows cations to flow through the central pore.[5] Two hydrophobic rings formed by the conserved residues, the leucine (L-ring) and valine (V-ring) rings, approximately at the midpoint of M2, contribute to channel gating.

[†] Chinese Academy of Sciences.
[‡] Instituto de Investigaciones Bioquímicas de Bahía Blanca and UNESCO Chair of Biophysics & Molecular Neurobiology.
[§] East China University of Science and Technology.

(1) Barrantes, F. J. *The nicotinic acetylcholine receptor: Current views and future trends;* Springer-Verlag: Berlin/Heidelberg, Germany, and Landers Georgetown, TX, 1998.
(2) Barrantes, F. J. *Curr. Opin. Drug Discovery Dev.* **2003**, *6*, 620−632.
(3) Hucho, F.; Weise, C. *Angew. Chem., Int. Ed.* **2001**, *40*, 3100−3116.
(4) Corringer, P.-J.; Le Novere, N.; Changeux, J.-P. *Annu. Rev. Pharmacol. Toxicol.* **2000**, *40*, 431−458.
(5) Karlin, A. *Nat. Rev. Neuronsci.* **2002**, *3*, 102−114.
(6) Unwin, N. *J. Mol. Biol.* **1993**, *229*, 1101−1124.
(7) Ortells, M. O.; Lunt, G. G. *Protein Eng.* **1996**, *9*, 51−59.
(8) Le Novere, N.; Corringer, P. J.; Changeux, J. P. *Biophys. J.* **1999**, *76*, 2329−2345.
(9) Miyazawa, A.; Fujiyoshi, Y.; Unwin, N. *Nature* **2003**, *423*, 949−955.

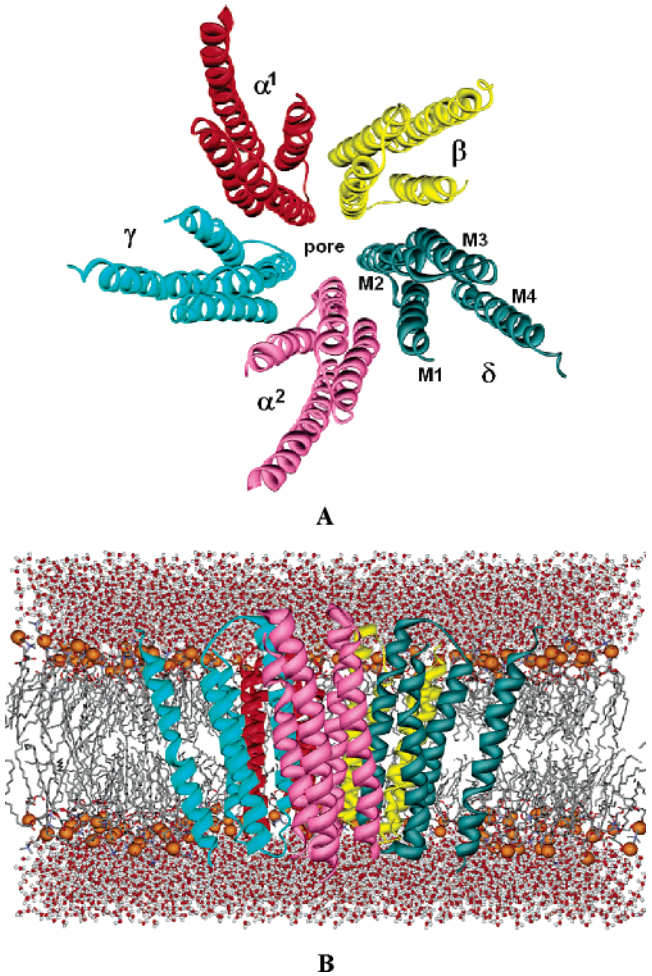

Figure 1. (A) Top view of the AChR transmembrane region (TM), as seen from the synaptic cleft, with subunits shown in different colors. To distinguish between the two α subunits, they are labeled α^1 and α^2. (B) Side view of the simulation system. The protein is drawn as ribbon, phosphate atoms of lipid are shown as brown balls, and the other atoms of the lipid are represented as sticks. Water molecules are displayed as balls and sticks. The front half of the bilayer is not shown for the sake of clarity.

This in turn leads to the opening and subsequent closing of the ion-permeation pathway.[3,5,9] It has been suggested that five M2 helices bend near the L-ring and twist around the pore axis in response to the binding of acetylcholine, which results in a conformational transition from a closed to an open channel.[10] Additionally, mutational and labeling experiments support the conclusion that interactions at the outermost M4 lipid-contacting ring[2] and internal TM segmental motions also contribute to the regulation of the gating mechanism.[4]

In the present study, the conformational dynamics of the whole TM domain of the AChR in dipalmitoylphosphatidylcholine (DPPC) lipid bilayers has been investigated using molecular dynamics (MD) simulations. Although simulations have been performed by other groups with a view to elucidating the properties of the ion channel, these previous studies only focus on the behavior of the pore-lining helix (M2) because of the structural limitations of the whole TM domain.[11−17] Our MD study extends the simulation to include both the intermediate M1−M3 ring and the outermost lipid-facing M4 ring.[2] The simulation results show asymmetrical and asynchronous structural motions of the subunits that can be considered "breathing" motions of the TM region. The nonbonded interactions of the outermost M4 TM ring with the rest of the TM segments on one hand, and with lipid molecules on the other, constitute the link between the structural dynamics of the channel and the lipid environment. Significantly, examination of the motions and conformational stability of the five M2 segments in the inner ring and of the minimal pore radius near the gating positions provides a detailed basis for analyzing the gating mechanism of the channel.

Methods

Simulation System. The cryoelectron crystallographic structure of the whole AChR TM domain was used as a starting structure for the simulations (PDB code, 1OED).[9] A large DPPC bilayer containing 512 lipid molecules was constructed by replicating an equilibrated block with 128 DPPC lipids four times. More than 100 lipids were subsequently removed from the constructed bilayer to generate a suitable membrane system into which the TM domain of the AChR could be embedded (Figure 1B). The protein/DPPC system was then solvated in a bath of SPC water molecules.[18] The resulting system was submitted to energy minimization to remove unfavorable contacts and equilibrated for 1 ns with positional restraints on the protein atoms. One Na^+ ion was subsequently added to compensate for the net positive charge of the system. Finally, the total system comprised 80 287 atoms.

MD Simulation. MD simulations were carried out with a GROMACS package,[19,20] using NPT and periodic boundary conditions. A modification of GROMOS87 force field [21] was applied for protein and the lipid parameters adopted were those used in previous MD studies of lipid bilayers.[22−25] The LINCS method [26] was used to constrain bond lengths, allowing an integration step of 2 fs. The structures for analysis were saved every 500 steps (1ps). Electrostatic interactions were calculated with the particle-mesh Ewald algorithm.[27,28] A constant pressure of 1 bar was applied independently in *X*, *Y*, and *Z* directions

(10) Unwin, N. *Nature* **1995**, *373*, 37−43.
(11) Kessel, A.; Shental-Bechor, D.; Haliloglu, T.; Ben-Tal, N. *Biophys. J.* **2003**, *85*, 3431−3444.
(12) Kessel, A.; Haliloglu, T.; Ben-Tal, N. *Biophys. J.* **2003**, *85*, 3687−3695.
(13) Sankararamakrishnan, R.; Adcock, C.; Sansom, M. S. P. *Biophys. J.* **1996**, *71*, 1659−1671.
(14) Law, R. J.; Forrest, L. R.; Ranatunga, K. M.; Rocca, P. L.; Tieleman, D. P.; Sansom, M. S. P. *Proteins: Struct. Funct. Genet.* **2000**, *39*, 47−55.
(15) Law, R. J.; Tieleman, D. P.; Sansom, M. S. P. *Biophys. J.* **2003**, *84*, 14−27.
(16) Adcock, C.; Smith, G. R.; Sansom, M. S. P. *Eur. Biophys. J.* **2000**, *29*, 29−37.
(17) Beckstein, O.; Biggin, P. C.; Bond, P.; Bright, J. N.; Domene, C.; Grottesi, A.; Holyoake, J.; Sansom, M. S. P. *FEBS Lett.* **2003**, *555*, 85−90.
(18) Berendsen, H. J. C.; Postma, J. P. M.; van Gunsteren, W. F.; Hermans, J. Interaction models for water in relation to protein hydration. In *Intermolecular Forces;* Pullman, B., Ed.; Reidel: Dordrecht, The Netherlands, 1981; pp 331−342.
(19) Berendsen, H. J. C.; van der Spoel, D.; van Drunen, R. *Comput. Phys. Commun.* **1995**, *91*, 43−56.
(20) Lindahl, E.; Hess, B.; van der Spoel, D. *J. Mol. Model.* **2001**, *7*, 306−317.
(21) (a) van Gunsteren, W. F.; Berendsen, H. J. C. *Gromos-87 manual*; Biomos BV: Groningen, The Netherlands, 1987. (b) van Buuren A. R.; Marrink, S. J.; Berendsen, H. J. C. *J. Phys. Chem.* **1993**, *97*, 9206−9212. (c) van Gunsteren, W. F.; Billeter, S. R.; Eising, A. A.; Hunenberger, P. H.; Kruger, P.; Mark, A. E.; Scott, W. R. P.; Tironi, I. G. *Biomolecular Simuulations: The GROMOS96 Manual and User Guide*; Vdf Hochschulverlag AG an der ETH Zurich: Zurich, Switzerland, 1996.
(22) Tieleman, D. P.; Sansom, M. S. P.; Berendsen, H. J. C. *Biophys. J.* **1999**, *76*, 40−49.
(23) Berger, O.; Edholm, O.; Jahnig, F. *Biophys. J.* **1997**, *72*, 2002−2013.
(24) Marrink, S. J.; Berger, O.; Tieleman, P.; Jahnig, F. *Biophys. J.* **1998**, *74*, 931−943.
(25) Tieleman, D. P.; Berendsen, H. J. C.; Sansom, M. S. P. *Biophys. J.* **1999**, *76*, 1757−1769.
(26) Hess, B.; Bekker, B.; Berendsen, H. J. C.; Fraaije, J. G. E. M. *J. Comput. Chem.* **1997**, *18*, 1463−1472.
(27) Darden, T. A.; York, D. M.; Pedersen, L. G. *J. Chem. Phys.* **1993**, *98*, 10089−10092.
(28) Essmann, U.; Perera, L.; Berkowitz, M. L.; Darden, T.; Lee, H.; Pedersen, L. G. *J. Chem. Phys.* **1995**, *103*, 8577−8592.

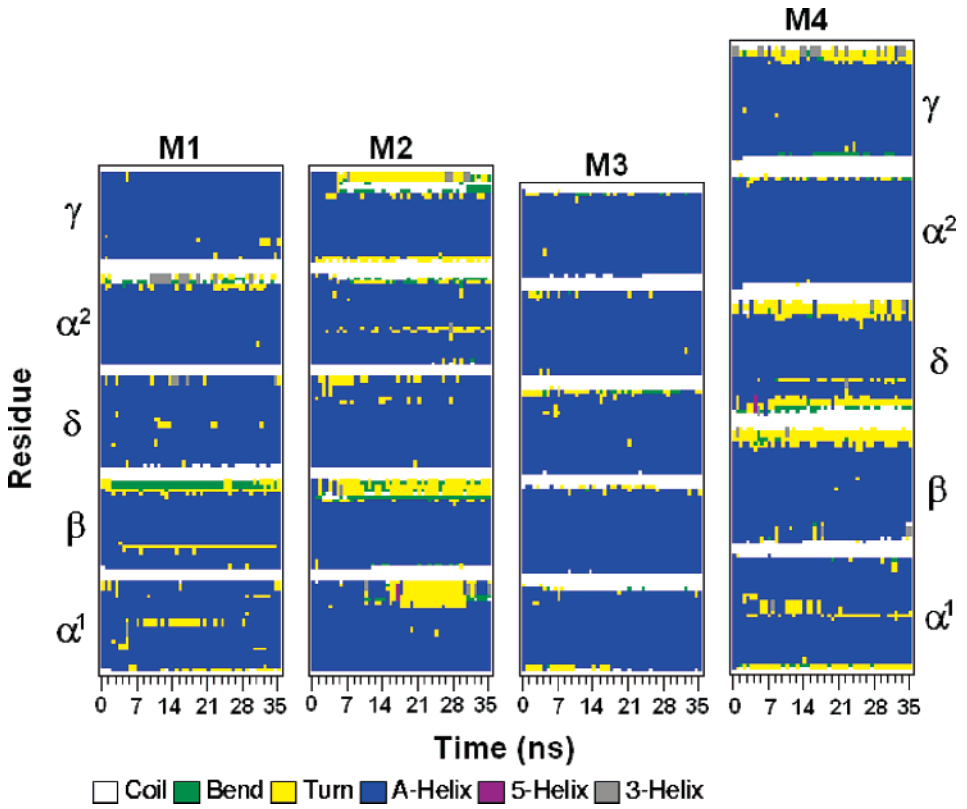

Figure 2. Secondary structure, analyzed using DSSP, as a function of time for TM segments $M1_{(5)}$, $M2_{(5)}$, $M3_{(5)}$, and $M4_{(5)}$. The structures were examined every 700 ps.

of the whole system with a coupling constant of 1.0 ps.[29] Water, lipids, and protein were coupled separately to a temperature bath at 323 K using a coupling time of 0.1 ps.[29]

MD simulations were run on a 128-CPU Silicon Graphics (Mountainview, CA) Origin3800 server. Analyses were performed using facilities within the GROMACS package. Secondary structure analysis employed the DSSP (define secondary structure of proteins) definitions.[30] Pore radius profiles were calculated using the HOLE program.[31−33] Structural diagrams were prepared using WebLab (http://molsim.vei.co.uk/weblab/) and PovRay (http://www.povray.org).

Results

A 35-ns simulation trajectory was used to analyze the conformational dynamics of the whole TM domain of AChR in DPPC bilayers. As shown in Figure S1 in the Supporting Information, the temperature fluctuations of the whole simulation system, the potential energy, and the main-chain root-mean-square deviation (RMSD) of the channel all indicate that the structure of the whole channel entered into equilibration after ~4 ns. The dynamic analyses of channel behavior are therefore focused mainly on the simulation period of 5−35 ns. For reasons of clarity, when referring to TM segments from all five subunits, we use the nomenclature $M1_{(5)}$, $M2_{(5)}$, $M3_{(5)}$, $M4_{(5)}$, and $M1-M3_{(5)}$, whereas in the case of a TM segment from a single subunit, e.g. α^1, the notation α^1M1 is used. All the time series data were smoothed over 500-ps intervals.

Secondary Structure Analysis. The time-dependent secondary structures of $M1_{(5)}$, $M2_{(5)}$, $M3_{(5)}$, and $M4_{(5)}$ were analyzed first (Figure 2). Overall, the TM segments retain a largely α-helical structure throughout the duration of the 35-ns simulation, with partial losses of α-helicity at the two ends of or within some TM segments. For example, approximately 5, 17, 3, and 16% of the α-helicity was lost at 35 ns with respect to the starting structure for $M1_{(5)}$, $M2_{(5)}$, $M3_{(5)}$, and $M4_{(5)}$, respectively. It was further found that the α-helical structure of $M2_{(5)}$ is not as stable as that of $M3_{(5)}$, which maintains the fixed α-helical conformation over the entire course of the simulation. In addition, the stability at a given location of the α-helical structure was found to be different for the TM segments of the different subunits, showing for instance γM1 to be the most stable of all $M1_{(5)}$ TM helices. On the basis of these analyses, it is concluded that the main secondary structure adopted by all TM segments in a DPPC bilayer is the α-helix, although the detailed distribution of the α-helical structure for each TM segment fluctuates according to the location in the protein. Moreover, the partial loss of α-helicity within the TM segment increases the flexibility of the TM helix in the lipid bilayer, as also reflected in the conformation changes of $M2_{(5)}$ discussed below.

Motions of M1−M3. In the starting structure, short connecting loops link M1−M2 and M2−M3, whereas the extended loop between M3 and M4 is missing. This led us to take three TM segments M1, M2, and M3 for each subunit as an integral domain (M1−M3) for the analysis. In Figure 3 the Cα RMSDs of $M1_{(5)}$, $M2_{(5)}$, $M3_{(5)}$, $(M1-M3)_{(5)}$, and M1−M3 for each subunit are plotted relative to the starting structure, and the snapshot structures of $(M1-M3)_{(5)}$ at the beginning, 10, 20, and

(29) Berendsen, H. J. C.; Postma, J. P. M.; van Gunsteren, W. F.; DiNola, A.; Haak, J. R. *J. Chem. Phys.* **1984**, *81*, 3684−3690.
(30) Kabsch, W.; Sander, C. *Biopolymers* **1983**, *22*, 2577−2637.
(31) Smart, O. S.; Goodfellow, J. M.; Wallace, B. A. *Biophys. J.* **1993**, *65*, 2455−2460.
(32) Smart, O. S.; Neduvelil, J. G.; Wang, X.; Wallace, B. A.; Sansom, M. S. P. *J. Mol. Graphics* **1996**, *14*, 354−360.
(33) Smart, O. S.; Breed, J.; Smith, G. R.; Sansom, M. S. P. *Biophys. J.* **1997**, *72*, 1109−1126.

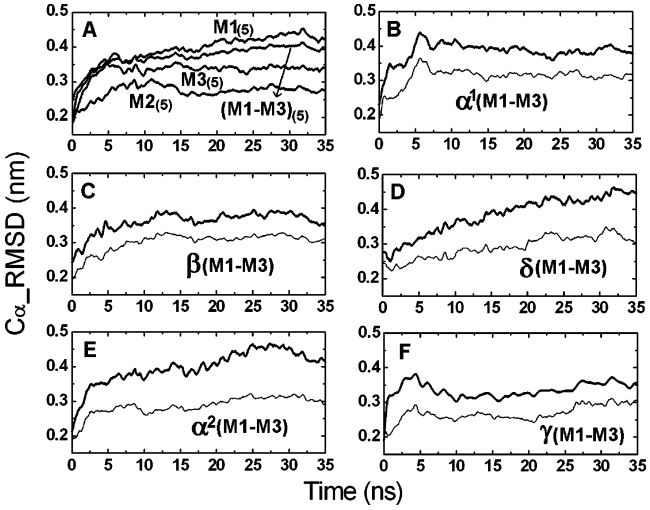

Figure 3. Time dependence of Cα RMSD with respect to the starting structure. Two models were fitted, one corresponding to Cα atoms of the M1−M3$_{(5)}$ bundles of the five subunits (thick line) and the other corresponding to Cα atoms of the M1−M3 bundles of each individual subunit (thin line). (A) Cα RMSDs of M1$_{(5)}$, M2$_{(5)}$, M3$_{(5)}$, and M1−M3$_{(5)}$. (B−F) Cα RMSDs of α^1(M1−M3), β(M1−M3), δ(M1−M3), α^2(M1−M3), and γ(M1−M3), respectively.

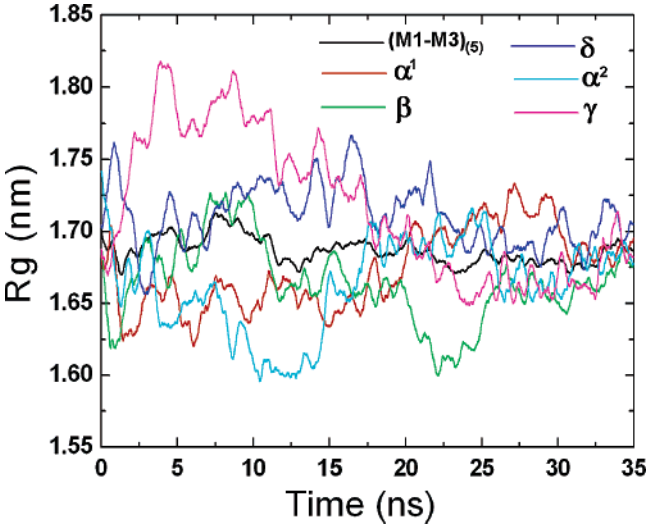

Figure 4. R_g for Cα atoms of (M1−M3)$_{(5)}$ and each M1−M3 relative to the axis of the channel.

35 ns, are shown in Figure S2 in the Supporting Information. As seen in Figure 3A, the RMSD of M1$_{(5)}$ increased steadily up to ∼0.45 nm over the first 32 ns and then decreased slightly during the last 3 ns. A similar behavior was observed for (M1−M3)$_{(5)}$. In contrast, the RMSD for M2$_{(5)}$ and M3$_{(5)}$ first ascended and then reached a plateau at ∼0.27 and ∼0.35 nm, respectively. These results suggest that M2$_{(5)}$, the inner wall of the channel, is more stable than M3$_{(5)}$ or M1$_{(5)}$. M1$_{(5)}$ fluctuated considerably more than M3$_{(5)}$ throughout the entire duration of the simulation. On the basis of the same model, differences in the calculated Cα RMSD of M1−M3 from each subunit were also apparent (Figure 3B−F). The overall RMSDs of β(M1−M3) and γ(M1−M3) were lower than those of the other three M1−M3s. Moreover, the noticeable difference in RMSD based on two different fitted models reflects not only that conformational changes have occurred but also that each M1−M3 has undergone translational or rotational motions, the magnitude of such motions being larger for α^2(M1−M3) and δ(M1−M3) than for the others. The measurement of Cα RMSD thus shows that different TM segments undergo different conformational fluctuations and motions during the course of the simulation, even though the sequence of each subunit is similar and the position of the five subunits in the starting structure is pseudosymmetrical.

To confirm the motions of each M1−M3 inferred from the Cα RMSD measurements, the translation of the Cα atoms of each M1−M3 was examined (Figure 4). The radius of gyration, R_g, calculated on the *XY* plane of the channel perpendicular to the pore axis (*Z* axis), was applied to measure the translation of each M1−M3. R_g is defined as

$$R_g = (\sum_i m_i r_i^2 / \sum_i m_i)^{1/2}$$

$$r_i^2 = (x_i - x_{com})^2 + (y_i - y_{com})^2$$

where m_i is the mass of the atom, x_i and y_i are the coordinates of the atom, and x_{com} and y_{com} are the coordinates of the centroid of (M1−M3)$_{(5)}$. Figure 4 shows that the R_g of (M1−M3)$_{(5)}$ always remained at ∼1.68 nm, becoming smoother as the simulation continued. In contrast, the R_g of each M1−M3, which contributes to the R_g of (M1−M3)$_{(5)}$, underwent a remarkable change along the 35-ns simulation, the R_g of γ(M1−M3) for instance increasing rapidly to ∼1.84 nm during the first 5 ns and then receding gradually to approach the R_g of (M1−M3)$_{(5)}$. This strongly suggests that γ(M1−M3) first moves outward and then comes back again to its original position. α^2(M1−M3) on the other hand followed the opposite trajectory. Finally, β(M1−M3) adopted a unique motional mode: first it moved outward, then inward, and finally outward again toward the end of the simulation. These outward and inward motions of α^1(M1−M3) and δ(M1−M3) are slightly smaller than those of the other M1−M3 segments. It is thus evident that the translation of each M1−M3 is asymmetrical and asynchronous during the 35-ns simulation. However, regardless of the motion adopted by each M1−M3, after 26 ns the R_g always approached that of (M1−M3)$_{(5)}$, causing the R_g of (M1−M3)$_{(5)}$ to become smoother toward the end of the simulation. By the end, the five M1−M3s had formed a pseudosymmetrical structure similar to that of the starting structure, despite the fact that the pseudosymmetry of (M1−M3)$_{(5)}$ had broken during the simulation.

The backbone (Cα atoms) rotation of each M1−M3 around an axis through its centroid and parallel to the channel pore axis was also examined. The time-dependent angle of rotation of each M1−M3 relative to its starting orientation is depicted in Figure S3 in the Supporting Information. The positive angle indicates that M1−M3 rotates counterclockwise around its axis. The exception to this is β(M1−M3) (see below). The angle of rotation of α^2(M1−M3) and γ(M1−M3) first increased to ∼9°, then slightly decreased, and finally increased again to a plateau value of ∼12°. After quickly rotating within the first 10 ns, α^1(M1−M3) and δ(M1−M3) maintained a rotating angle of ∼6° throughout the rest of the simulation. β(M1−M3) was the only segment to adopt a clockwise rotation during part of the 35-ns simulation: it began in a clockwise direction, reversed to a counterclockwise direction after ∼23 ns, and then returned to its starting position at 35 ns. As with the translational motions, rotations vary among different TM segments.

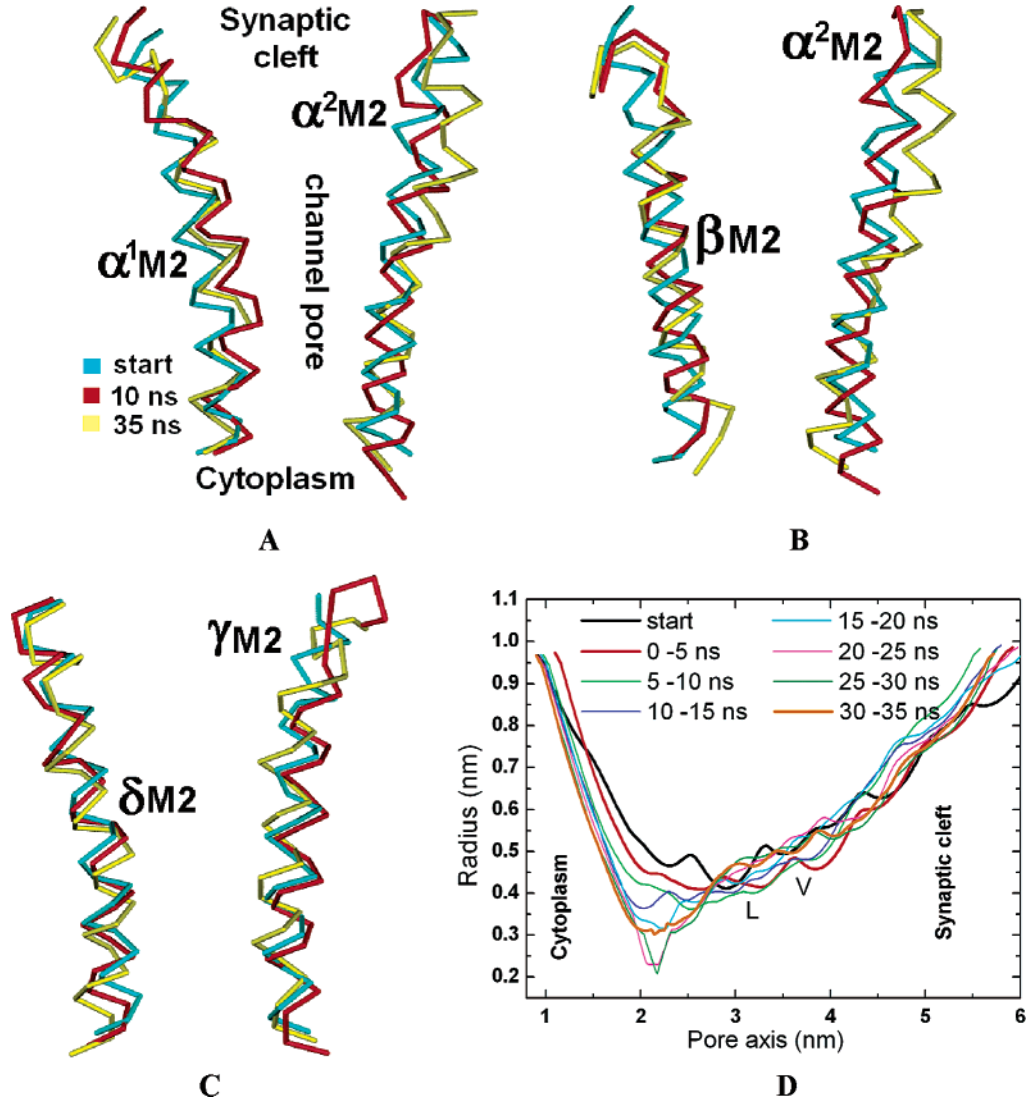

Figure 5. (A−C) Cα snapshots at $t = 0$, 10, and 35 ns of M2 superimposed by fitting all Cα atoms of $M2_{(5)}$. (D) Pore radius profiles vs position along the pore axis. Eight curves were produced on the basis of Cα atoms of $M2_{(5)}$ from the starting structure and seven averaged structures extracted from the 35-ns trajectory.

Since M2 constitutes the inner wall of the channel and its conformational changes or motions directly affect the shape of the pore, particular attention was paid to the dynamic behavior of the inner ring. The time-dependent R_g of $M2_{(5)}$ shows that the channel pore consisting of $M2_{(5)}$ became enlarged by about 0.05 nm with respect to the initial structure after 7 ns (Figure S4 in the Supporting Information). Individually, α^1M2 increased from ∼1.02 to ∼1.15 nm (Figure S4), constituting the main contribution to the expansion of $M2_{(5)}$. Though the other four M2s deviate from their starting value, they finally reach positions close to the initial ones. The superimposed snapshots obtained by fitting all Cα atoms of $M2_{(5)}$ displayed in Figure 5A−C reflect the conformational change of each M2 along the 35-ns simulation. The bend at the midpoint of α^1M2 became more marked at 10 ns but then reverted to its original form at 35 ns (Figure 5A). The α^2M2 bend was flexible, allowing half of the α^2M2 helix near the synaptic cleft to deviate from the pore axis and the helix near the cytoplasmic surface of the membrane to move toward the pore axis (Figure 5B). βM2 held a similar conformation at its starting structure except for the cytoplasmic end of this helix, which moved toward the pore (Figure 5B). Thus the motion of α^2M2 and βM2 helices near the cytoplasm considerably reduces the pore radius near the cytoplasmic vestibule. The small conformational fluctuation of δM2 had almost no effect on the shape of the pore (Figure 5C). In the case of γM2, although it bent like α^1M2, the original conformation was not restored within 35 ns. Taken together, the conformations of the innermost ring formed by the M2 TM segments show that the backbone of M2 is flexible and that such flexibility changes the shape of the channel pore.

Having examined the conformational changes, translations, and rotations of $(M1-M3)_{(5)}$ and $M2_{(5)}$, we analyzed how these structural dynamics act to shape the channel pore. The pore can be characterized in terms of its pore radius profile.[15,31−33] Figure 5D displays the pore radius profiles based on the Cα atoms of $M2_{(5)}$, revealing how the backbone of the pore changes during the 35-ns simulation. In the starting structure, the minimum radius of the channel pore (∼0.4 nm) is near the L-ring. The average pore radius profile over the course of the initial 5 ns is similar to that of the starting structure. However, as the simulation continued, the pore radius near the cytoplasmic end became smaller and smaller. The minimum radius during

the initial 20−30 ns approached ∼0.2 nm. According to the snapshots in Figure 5B, this is caused by the conformational switch of βM2 and α^2M2. During the last 5 ns of the simulation, the minimum radius was restored to ∼0.3 nm, i.e., close to the value at 15−20 ns. This is the converse of the behavior at the narrow end of the pore, located at the cytoplasmic side of the membrane. The widest region of the pore is located at the synaptic end. It increased in diameter during the 35-ns simulation, which explains why the R_g of $M2_{(5)}$ increased ∼0.05 nm with respect to the initial structure (Figure S4). Furthermore, the radius changed at the two ends of the pore; the average profiles for the main body of the pore (∼0.28−5.4 nm along the pore axis) extracted from the simulation data were very similar to the value in the starting structure. Without taking into consideration the residue side chains, the dynamics of the structure therefore causes the two ends of the pore to enlarge or contract, with no distinct changes being observed in the pore from ∼2.8 to 5.4 nm along the pore axis.

Size of the Gate. The backbone size of the pore near the two gate positions, the leucine-ring (L-ring) and the valine-ring (V-ring), maintained its initial value almost unaltered for the duration of the 35-ns simulation (Figure 5D). However, previous studies have shown that side-to-side interactions bring together the side chains of the L (or V) residues from each subunit to form a tight hydrophobic girdle around the pore, preventing the ions from passing through when the channel is closed.[3,9] Side-chain motions at the pore axis and the minimal pore radius near the L-ring and V-ring were therefore analyzed next. Two angles, Cγ— Cα—COM for the L-ring and Cβ — Cα—COM for the V-ring, were defined to reflect the side-chain motion of each residue. Cγ, Cα, and Cβ are the atoms of residues and COM is the centroid of Cα atoms from five residues in the L-ring or the V-ring. Side-chain atoms were taken into account for the calculation of the minimal pore radius.

As shown in Figure S5 in the Supporting Information, the angle of Cγ— Cα—COM in residue α^1L quickly increased to ∼100° and then rapidly diminished again during the first 2 ns, suggesting that the side chain of residue α^1L shifts rapidly away from the pore axis at the beginning of the simulation and then returns to its initial position. The angle in residue βL indicates that its side chain already deviates from the pore axis in the starting structure, a conformation which is retained over the whole 35-ns simulation. A similar behavior was observed for residue α^2L. However, such motion induces the side chain of residue δL to point toward the pore axis at the end of the simulation. The side chain of residue γL also pointed toward the pore axis, although there was a small deviation during the simulation. The final outcome of the side-chain motions of the five L residues is that the minimal pore radius near the L-ring increases from ∼0.3 to ∼0.4 nm during the first 2 ns and is subsequently held at ∼0.3 nm until the end of the simulation (Figure 6).

At variance with the L-ring, the side chains of the V-ring in the starting structure all pointed toward the pore axis (Figure S6 in the Supporting Information). However, except for residue α^2V, the side chains of the other four residues deviated to variable extents from the pore axis during the simulation, resulting in a gradual increase in the minimal pore radius near the V-ring, which reached ∼0.6 nm at ∼31 ns (Figure 6). It is therefore conjectured that the side-chain motion leads to a

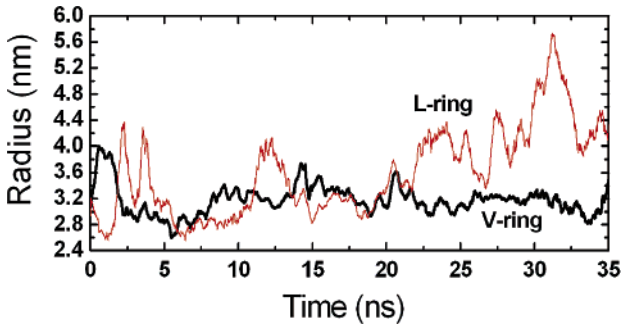

Figure 6. Time-dependent minimal pore radius near the L-ring and V-ring.

closed-to-open gating mechanism in the V-ring during the time window of the 35-ns simulation, such conformational switch arising from side-chain rotations of α^1V, βV, δV, and γI residues.

Motions of M4. The fourth segment of each subunit, M4, located at the outermost layer of the TM region, is particularly important since it establishes more interactions with neighboring lipid molecules than any other TM segment and is totally secluded from contact with the AChR pore region proper.[2] For the purpose of exploring the orientation adopted by each individual M4 segment during the simulation we considered the angle between the axis of each M4 helix and the *Z*-axis (i.e. the axis perpendicular to the plane of the bilayer) as the tilt angle of the TM helix. Figure 7A shows the change in the tilt angle of each M4 segment in the simulation as a function of time. At time zero each M4 helix was positioned at ∼20°, after which the tilt angle of α^1M4 increased rapidly to ∼35° during the first 3 ns, and subsequently fluctuated around ∼30° for the remainder of the simulation. In the case of βM4 the increase in the tilt angle was much smaller and the helix returned to its initial orientation at the end of the simulation. The δM4 helix gradually tilted away from the *Z*-axis and reached a final tilt angle of ∼30°. A similar change of orientation was observed for α^2M4. For γM4, the tilt angle reached a value of ∼27° within 3 ns and fluctuated around this value during the rest of the simulation. Hence, each M4 helix deviates from its initial position within the time frame of the 35-ns simulation, although the degree of tilt is rather different for each one. Furthermore, the superimposition of $M4_{(5)}$ at 0 and 35 ns in Figure 7B reveals that $M4_{(5)}$ tilted concertedly in a clockwise direction.

Discussion

A 35-ns MD simulation was carried out on the basis of a cryoelectron crystallographic structure (PDB code, 1OED[9]) to explore the dynamic conformations that occur in the whole TM domain of the AChR as it relaxes in the lipid bilayer. Since the cryoelectron microscopy structure was constructed at 4-Å resolution,[9] a relatively long MD simulation is helpful to refine the structure of 1OED. Simulation of the whole TM domain of the AChR further enabled us to examine contributions from TM segments other than the inner ring, channel-lining segment M2, as in previous simulations.[14,15] Channel opening triggered by ACh binding could naturally not be tested in the present study since only the TM domain was used, and the simulation time frame is far from the time scale required for the channel to undergo closed↔open transitions in the physiological time domain.

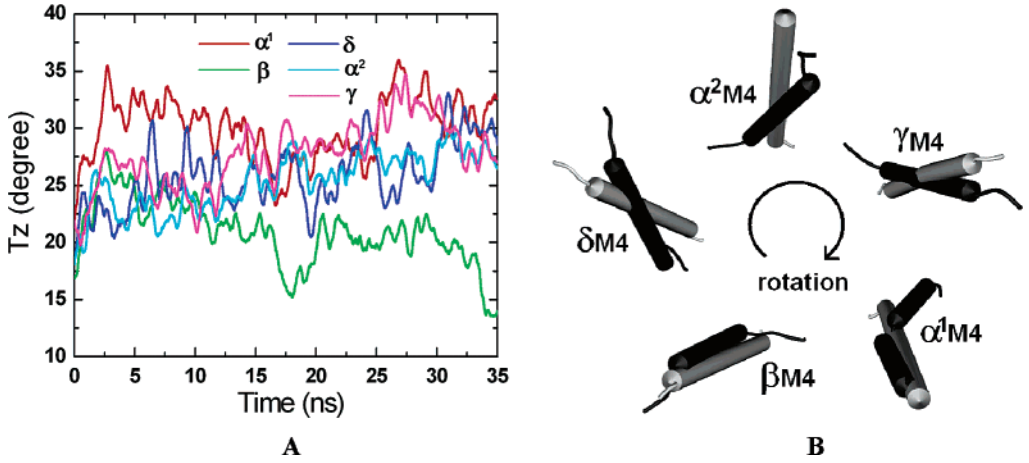

Figure 7. (A) Time-dependent tilt angle between each M4 helix and the normal of the DPPC bilayer (*Z* axis). The Cα atom centroids of residues 7−10 and 26−29 are set as the top and bottom of the axis of each M4 helix, respectively. (B) Cα snapshots at $t = 0$ (gray) and 35 ns (black) of the five M4 segments were superimposed by fitting all Cα atoms of $M4_{(5)}$.

The DSSP analysis of $M1_{(5)}$, $M2_{(5)}$, $M3_{(5)}$, and $M4_{(5)}$ structure (Figure 2) shows the major secondary structure of all the TM segments to be α-helix, with no β-sheet being formed at any time during the simulation. This observation validates the rationality of the cryoelectron crystallographic structure[9] but goes against the previous hypothesis[6−8] that the TM region of AChR adopts a predominantly mixed α/β topology. The strong α-helical character of the TM segments reflected in the simulation is consistent with previous biophysical and/or biochemical studies of the individual TM segment or the intact AChR[9,34−41]. Moreover, the partial loss of the α-helicity occurred not only at the extremities but also within some TM segments. The α-helix to bend or turn switch within the TM segment led to the formation of flexible hinges within the helix, which may be associated with conformational changes of the M2 and M4 helices (Figures 5 and 7). The flexibility of the TM helix induced by the secondary structure switch, in particular for the M2 helix, may be directly related to the ion-permeation function of the channel. Secondary structure examination of the channel during the simulation therefore brings out potentially functional conformations of the channel.

In addition, the results of the 35-ns simulation show an asymmetrical and asynchronous motion for $M1-M3_{(5)}$ from the five subunits. During the translation of $M1-M3_{(5)}$, γM1−M3, and δM1−M3 move away from the pore axis as α^1M1−M3 and α^2M1−M3 move toward it, temporarily resulting in an asymmetrical structure of $M1-M3_{(5)}$ (Figure 4). Remarkably, after about 30-ns MD simulation, the relative location of each M1−M3 in $M1-M3_{(5)}$ is very similar to the starting structure and a pseudosymmetrical structure is again formed (Figure 4). It is thus postulated that the $M1-M3_{(5)}$ transmembrane segments undergo some kind of "breathing" (local expansion or contraction) motion in the time scale of the simulation. Furthermore, each individual M1−M3 rotates in different directions and to varying extents (Figure S3). At variance with what happens in the case of translational motions, only βM1−M3 rotates back to the initial position at the end of the simulation; the other four M1−M3 segments all reach new positions. The rearrangement of the five M1−M3 caused by the rotation of each M1−M3 suggests the existence of incompatible interactions among the five M1−M3 domains in the starting structure.

Asymmetrical motion has also been observed for the five M2 helices, their conformational changes also being asymmetrical and asynchronous. For example, whereas βM2 adopted a linear helix structure, the kink in α^1M2 increased (Figure 5A−C). As a consequence, the backbone size of the pore did not change much except at the two ends. We thus postulate that the five M1−M3s, and in particular the five M2 helices in the inner ring, only undergo symmetrical and synchronous motions—or conformational fluctuations—such as the bending occurring in all five M2 helices, so that the backbone of the channel pore subsequently expands or contracts with relatively larger motions. Obviously, the 35-ns simulation period is not long enough to catch the full structural transitions of closed-to-open conformational changes associated with ion permeation through the pore, which occur in the microsecond time scale, but the V-ring conformational switch already apparent in the time window of the MD simulation may be related to the preceding, much faster, gating mechanism. Although no significantly large changes were observed in the backbone of the pore within the 35-ns duration, the motions and the flexibility of the five M2 helices made apparent by the simulation partially support the previous hypothesis that they are able to bend near the L-ring and twist around the pore axis to open the channel.[10]

Although the connecting loop between M3 and M4 in each AChR subunit is missing in the AChR TM domain used in the simulations, the calculated Lennard-Jones potential energies (Figure 8) as a function of simulation time indicate that some van der Waals interactions exist between $M1-M3_{(5)}$ and $M4_{(5)}$. These interactions are strongest near 10 ns, which corresponds to the largest translational motions in $M1-M3_{(5)}$. Subsequently, as the structure of $M1-M3_{(5)}$ gradually reverts to its previous pseudosymmetrical structure, the van der Waals interactions between $M1-M3_{(5)}$ and $M4_{(5)}$ also return to their initial

(34) Methot, N.; Ritchie, B. D.; Blanton, M. P.; Baenziger, J. E. *J. Biol. Chem.* **2001**, *276*, 23726−23732.
(35) Blanton, M. P.; Cohen, J. B. *Biochemistry* **1994**, *33*, 2859−2872.
(36) Tamamizu, S.; Guzman, G. R.; Santiago, J.; Rojas, L. V.; McNamee, M. G.; Lasalde-Dominicci, J. A. *Biochemistry* **2000**, *39*, 4666−4673.
(37) Methot, N.; Baenziger, J. E. *Biochemistry* **1998**, *37*, 14815−14822.
(38) Corbin, J.; Methot, N.; Wang, H. H.; Baenziger, J. E.; Blanton, M. P. *J. Biol. Chem.* **1998**, *273*, 771−777.
(39) Opella, S. J.; Marassi, F. M.; Gesell, J. J.; Valente, A. P.; Kim, Y.; Oblatt-Montal, M.; Montal, M. *Nat. Struct. Biol.* **1999**, *6*, 374−379.
(40) Lugovskoy, A. A.; Maslennikov, I. V.; Utkin, Y. N.; Tsetlin, V. I.; Cohen, J. B.; Arseniev, A. S. *Eur. J. Biochem.* **1998**, *255*, 455−461.
(41) Pashkov, V. S.; Maslennikov, I. V.; Tchikin, L. D.; Efremov, R. G.; Ivanov, V. T.; Arseniev, A. S. *FEBS Lett.* **1999**, *457*, 117−121.

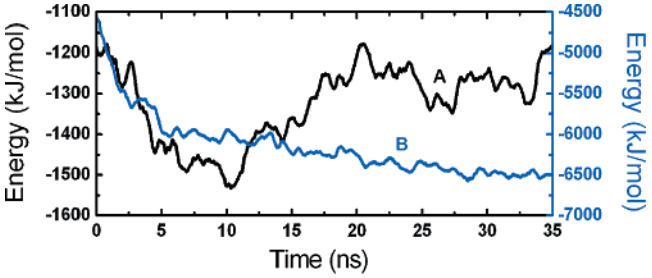

Figure 8. Time-dependent Lennard-Jones potential between $M1-M3_{(5)}$ and $M4_{(5)}$ (A) and between $M4_{(5)}$ and DPPC lipid molecules (B). The values of curves A and B correspond to the left and right *y*-axes, respectively.

state. This suggests that the nonbonded interactions between $M1-M3_{(5)}$ and $M4_{(5)}$ are related to the motions of $M1-M3_{(5)}$. Furthermore, the tilt angle of each M4 helix relative to the normal of the lipid bilayer shows that the $M4_{(5)}$ segments increase their hydrophobic interactions with the surrounding DPPC molecules by burying themselves deeper into the hydrophobic region of the bilayer. In concordance with the transition of the tilt angles, the van der Waals interactions between $M4_{(5)}$ and the DPPC lipids reflected by the Lennard-Jones interaction energy tend to be stronger along the simulation time and fluctuate slightly around −6500 kJ/mol after ∼30 ns (Figure 8). Moreover, the equilibration process for the $M4_{(5)}$−lipid interaction is slow. Therefore, the interactions of $M4_{(5)}$ with $M1-M3_{(5)}$ and lipid molecules, respectively, suggest that the outer ring of $M4_{(5)}$ acts as the vehicle to transfer the influences of the lipid surroundings to the conformation changes of the whole channel. This may explain why mutations in the outer ring residues of αM4, *β*M4, and *γ*M4 affect channel function[36,42,43] and how the lipid environment affects the stability of the functional states of the AChR,[44] as well as providing a rational explanation as to how several pharmacologically relevant ligands that partition in the lipid bilayer affect AChR channel function.[2]

The pore radius profile calculated on the basis of the Cα atom of $M2_{(5)}$ showed that the backbone size of the two "gating" positions, i.e., the L-ring and the V-ring, is close to that of the starting structure. However, considering the rearrangement of side chains of residues forming the L-ring and V-ring, the recalculated minimal pore radius near these two gating rings reveals that, near the end of the simulation, the narrowest region of the V-ring is almost double the size of the starting structure. This led us to assume that the reorganization of the side chains suffices to break the side-to-side hydrophobic girdle of the gate and thereby contribute to the closed-to-open conformational transition of the gating ring within the course of nanoseconds. Significantly, the estimation of the Cγ−Cα−COM angle in each L residue indicates that the side-to-side hydrophobic interactions of the L-ring are broken in the starting structure, because the side chains of *β*L and α^2L residues initially move far away from the pore axis. In contrast to what is observed with the V-ring, the minimal pore radius near the L-ring is always around the initial value throughout the entire simulation, except for a rapid jump within the first 2 ns. The reason for this singularity might be that α^1L, *δ*L, and *γ*L residues are located in a triangular disposition (Figure 1A) and their side chains all point to the pore axis, still effectively occluding the channel lumen. It is thus suggested that each of the five L residues participates independently and symmetrically in the structural transition between the closed and open states, a possibility that appears to be validated by independent mutagenesis experiments.[45] To obtain the absolute values for the opening of the L-ring, the side-chain deviations from the pore axis of all the five L residues are required. We observed that the backbone size near the V-ring is larger than the L-ring (Figure 5D), and the side chains of four residues simultaneously rotate away from the pore axis when the minimal pore radius near the V-ring reaches its maximal value. This might make it easier for the V-ring to act as the closed-to-open conformational switch than is the case with the L-ring.

Conclusions

The dynamic structural behavior of the whole TM domain of the AChR and a possible gating mechanism of the channel have been studied on the basis of a 35-ns MD simulation. The fixed α-helical structures of the 20 TM segments throughout the entire 35-ns simulation validate the overall rationality of the starting structure obtained from cryoelectron microscopy data and disprove previous hypotheses about the mixed α-helix/*β*-sheet topology of this region. The asymmetrical and asynchronous motions of the M1−M3 segments from each subunit have been explored, and from the motion of the five M4 TM helices one can infer that the latter play a unique role, probably transmitting signals from the membrane environment to the relatively distant M2 inner-ring (pore) region. The availability of isolated AChR TM peptides and larger proteolytic fragments containing the AChR TM region, together with site-directed fluorescence labeling techniques, should provide the time and spatial resolution required to explore the conformational transitions predicted in the present MD simulations. Finally, a gating mechanism is postulated whereby the side-chain arrangement of residues leads to the gating of the channel in a time scale of nanoseconds, whereas the subsequent motions of the backbone in the closed-to-open conformational transitions, occurring in the microsecond time domain, depend on the symmetrical and synchronous motions of the five subunits.

Acknowledgment. We thank Dr. Peter Tieleman for providing the initial coordinates of the DPPC bilayer and some MD simulation parameters, and Dr. Richard H. Henchman for help with the analysis of the rotation of TM domain. This work was supported by the State Key Program of Basic Research of China (Grant 2002CB512802), the National Natural Science Foundation of China (Grants 20372069, 29725203, and 20072042), the Basic Research Project for Talent Research Group from the Shanghai Science and Technology Commission, the Key Project from the Shanghai Science and Technology Commission (Grant 02DJ14006), the Key Project for New Drug Research from CAS, and the 863 Hi-Tech Programm (Grants 2002AA233061, 2001AA235051, 2001AA235041, 2002AA104270, 2002AA233011, and 2003AA235030). This work was also supported in part by grants from the Universidad Nacional del Sur, and FONCYT, Argentina.

(42) Lee, Y. H.; Li, L.; Lasalde, J.; Rojas, L.; McNamee, M.; Ortiz-Miranda, S. I.; Pappone, P. *Biophys. J.* **1994**, *66*, 646−653.
(43) Bouzat, C.; Bren, N.; Sine, S. M. *Neuron* **1994**, *13*, 1395−1402.
(44) daCosta, C. J. B.; Ogrel, A. A.; McCardy, E. A.; Blanton, M. P.; Baenziger, J. E. *J. Biol. Chem.* **2002**, *277*, 201−208.
(45) Labarca, C.; Nowak, M. W.; Zhang, H.; Tang, L.; Deshpande, P.; Lester, H. A. *Nature* **1995**, *376*, 514−516.

Supporting Information Available: Temperature of the whole simulation system, the potential energy, and the main-chain RMSD of the channel along the 35-ns simulation (Figure S1), four snapshots of M1−M3$_{(5)}$ along the 35-ns simulation (Figure S2), rotation of each M1−M3 (Cα atoms only) around its own axis during the entire 35-ns simulation (Figure S3), time-dependent R_g for Cα atoms of M2$_{(5)}$ and each individual M2 relative to the center axis of the channel pore (Figure S4), and side-chain motions of each residue in the L-ring and V-ring gating positions, respectively (Figures S5 and S6) (PDF). This material is available free of charge via the Internet at http://pubs.acs.org.

JA044577I